Harnessing Geometric Phase Metasurfaces to Double the Field of View in Polarized Structured Light Projection for Depth Sensing

Chia-Hsun Chang, Wen-Cheng Hsu, Chih-Ting Chang, You-Chia Chang, Chi-Wai Chow, *Senior Member, IEEE*, Hsin-Chieh Yu, Yao-Wei Huang, Gong-Ru Lin, *Fellow, IEEE*, Yu-Heng Hong, and Hao-Chung Kuo, *Fellow, IEEE*

***Abstract*—Herein, a lucid meta-holographic approach leveraging geometric phase metasurfaces and photonic crystal surface-emitting lasers is presented. Such a straightforward technique inherently enables polarized structured light projection with opposite circular polarization states, effectively doubling the field of view for depth sensing applications. Furthermore, the innate polarization state of projected light provides enhanced resistance to environmental interference. To demonstrate the practical utility of this method, an integrated depth sensing system based on the geometric phase meta-hologram has been developed and successfully detects targets at an operating distance of 75 cm, paving the way for advanced 3D sensing applications in various fields.**

***Index Terms*—Metasurface, *structured light*, *3D depth sensing*.**

I. Introduction

As the demand for spatial information acquisition continues to grow, three-dimensional (3D) surface imaging and mapping technology has emerged as a remarkable facilitator in various applications, such as machine vision, spatial computing for augmented/virtual reality (AR/VR), LiDAR [1], wearable devices [2], and autonomous driving. Laser-based 3D imaging systems [3], [4], [5] have demonstrated significant application potential in a wide range of devices. Moreover, the rapid development of nano-photonic technologies, driven by the pursuit of lightweight, compact, and high-performance characteristics, has brought metasurfaces to the forefront as a promising artificial optical platform. In contrast to traditional diffractive optical elements (DOEs), metasurfaces [6], [7] consist of a single layer of subwavelength meta-atoms, enabling unique light manipulation capabilities within a two-dimensional (2D) planar surface. This groundbreaking innovation effectively addresses the challenges associated with the inherent large volume and low angular efficiency of DOEs. The unique ability of the metasurface to control polarization enables free manipulation of spatial polarization, allowing for polarization encoding and analysis in image control [8], [9]. This enhances and diversifies the spatial image analysis capabilities of the metasurface.

Recent advancements have seen the demonstration of ultra-compact devices through the on-chip integration of vertical cavity surface emitting lasers (VCSELs) [10], [11], [12] and metasurfaces [13], [14], [15], [16]. However, the large divergence and limited single-mode output power of VCSELs have hindered their widespread adoption. In comparison, photonic crystal surface-emitting lasers (PCSELs) [17], [18], [19], [20] offer narrow divergence, symmetric beam profiles, and higher output power, making them a promising candidate for next-generation laser source integration solutions. The use of PCSELs eliminates the need for complex lens systems and precise adjustments, further streamlining the integration process and enhancing the overall performance of the resulting devices.

In this work, we demonstrate a meta-hologram [21], [22], [23] which can generate a multi-beam structured light (SL) projection [5], [24], [25]. Such a meta-hologram provides customized light beam distributions within the constraints of the periodic meta-atom arrangement, achieving a specific field of view (FOV). To further expand the FOV, we employ the geometric phase-based metasurfaces [26], [27]. This lucid approach enables the generation of symmetric left-circular polarization (LCP) and right-circular polarization (RCP) far-field light patterns, as illustrated in Fig. 1(a). The versatility of this technique allows for the creation of tailored far-field light distributions for specific

Manuscript received 23 June 2024; revised 11 July 2024; accepted 11 July 2024. Date of publication 16 July 2024; date of current version 25 July 2024. This work was supported by the National Science and Technology Council (NSTC) in Taiwan under Grant 110-2622-8-A49-008-SB, Grant 111-2622-8-A49-021-SB, Grant 110-2112-M-A49-034-MY3, and Grant 112-2740-M-A49-001. *(Chia-Hsun Chang and Wen-Cheng Hsu are co-first authors.) (Corresponding authors: Yu-Heng Hong; Hao-Chung Kuo.)*

Chia-Hsun Chang and Wen-Cheng Hsu are with the Department of Photonics, College of Electrical and Computer Engineering, National Yang Ming Chiao Tung University, Hsinchu 30010, Taiwan, and also with the Semiconductor Research Center, Hon Hai Research Institute, Taipei 11492, Taiwan (e-mail: joshua.ch.chang@foxconn.com; wen-cheng.hsu@foxconn.com).

Chih-Ting Chang and Yu-Heng Hong are with Semiconductor Research Center, Hon Hai Research Institute, Taipei 11492, Taiwan (e-mail: nicochang18@gmail.com; enoch.yh.hong@foxconn.com).

You-Chia Chang, Chi-Wai Chow, Yao-Wei Huang, and Hao-Chung Kuo are with the Department of Photonics, College of Electrical and Computer Engineering, National Yang Ming Chiao Tung University, Hsinchu 30010, Taiwan (e-mail: youchia@nycu.edu.tw; cwchow@nycu.edu.tw; ywh@nycu.edu.tw; hckuo@faculty.nctu.edu.tw).

Hsin-Chieh Yu is with the College of Photonics, Institute of Lighting and Energy Photonics, National Yang Ming Chiao Tung University, Tainan 711, Taiwan (e-mail: hcyu@nycu.edu.tw).

Gong-Ru Lin is with the Graduate Institute of Photonics and Optoelectronics and the Department of Electrical Engineering, National Taiwan University, Taipei 10617, Taiwan (e-mail: grlin@ntu.edu.tw).

Digital Object Identifier 10.1109/JPHOT.2024.3429348

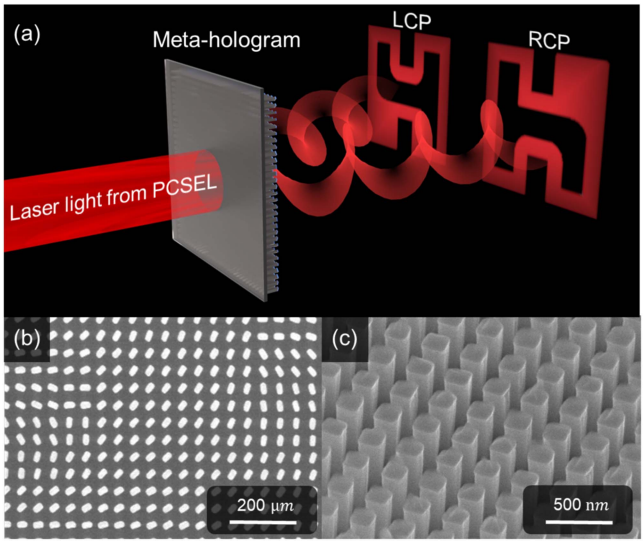

Fig. 1. (a) The schematic diagram illustrates a meta-hologram technique for reconstructing holographic images by leveraging a geometric phase metasurface and PCSEL. (b) The scanning electron microscope (SEM) image shows the top view of a fabricated geometric phase metasurface. (c) The close-up image of a fabricated propagation phase-based metasurface.

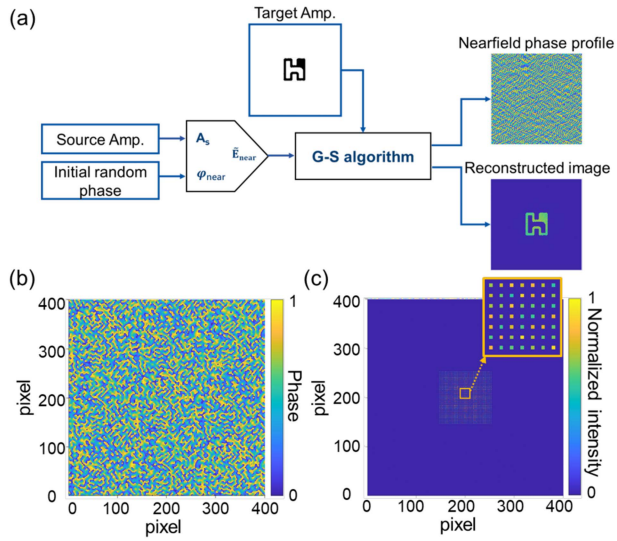

Fig. 2. (a) The flowchart depicts the iterative G-S algorithm. (b) Near-field phase of multi-beam SL projection within a FOV of 20° × 20°. (c) Calculated far-field pattern resulting from the designed near-field phase.

application requirements. By leveraging the geometric phase, we not only expand the original holographic FOV but also enable the reconstruction of SL projection with polarization states. This advancement opens new possibilities for the applications requiring both extended FOV and polarization control in SL projection systems.

II. Design Principle of Structure Light Meta-Hologram

In the meta-hologram design for multi-beam SL projection, the FOV plays a crucial role and is significantly influenced by the diffraction characteristics of the reconstructed image. This is particularly important in SL design as it directly affects the quality of projected light spots and the resolution of each pixel. These factors, in turn, determine the accuracy of sensing light spot distribution in depth sensing. Generally, the utilization of periodic nanostructures enables the realization of pixels, where a supercell is composed of n×n meta-atoms with a pitch p, and n×p represents the size Λ of each pixel. The diffraction angle of the meta-hologram, composed of these periodic pixel structures, can be described as:

$$\theta_{0\text{th}} = \sin^{-1}\left(\frac{\lambda}{2\Lambda}\right) \tag{1}$$

where λ is the wavelength, the FOV at the zero order is $\theta_{0\text{th}}\times 2$ [30], indicating that the holography exhibits a diffraction angle at the zero order. Additionally, according to the diffraction formula, the diffraction angles in the x and y directions for each pixel position are defined, described as:

$$\theta^{n}_{\text{pixel}} = \sin^{-1}\left(\frac{n\times\lambda}{m\times\Lambda}\right) \tag{2}$$

where n is the pixel order from the center point in the 2D plane, and m is the total number of pixels along a single axis of the hologram [22], representing the diffraction angle of any pixel in the hologram defined by the n order pixel. By utilizing the aforementioned diffraction angles in the x and y directions, we have the capability to arbitrarily control the beam angles within the range of the diffraction angles in the FOV.

Next, to obtain the phase distribution for the designed original image intensity, we utilized the iterative Fourier transform algorithm (IFTA) of computer-generated hologram, to retrieve the near-field phase, as shown in Fig. 2(a). The flowchart depicts the iterative Gerchberg-Saxton (G-S) algorithm [28], [29] employed for holographic reconstruction, which starts with the source amplitude and an initial random phase to compute the initial electric field. Then, the algorithm repeatedly incorporates the target amplitude to derive the required near-field phase as shown in Fig. 2(b). which undergoes Fourier transformation to obtain the far-field intensity. This far-field intensity is compared with the target intensity, and the iterative process continues until the convergence is achieved, yielding the desired holographic reconstruction, as shown in Fig. 2(c). The schematic presents the calculated far-field pattern resulting from the designed near-field phase. As shown in the inset, a detailed close-up view of the array of light points is provided, showcasing the intricate structure and precise arrangement of the projected light spots.

One of the designed phase distributions is to project holographic patterns, providing a multi-beam SL projection within a FOV of 20° × 20°, spanning a range of −10° to 10° in both the X and Y directions. Such an approach enables the realization of highly customizable and intricate light patterns for various applications in SL projection. Additionally, another design for the Hon Hai logo with the same FOV is implemented.

In the design of SL for holographic imaging, achieving higher spatial resolution can be facilitated by increasing the density of points within the same spatial spacing. However, it is essential

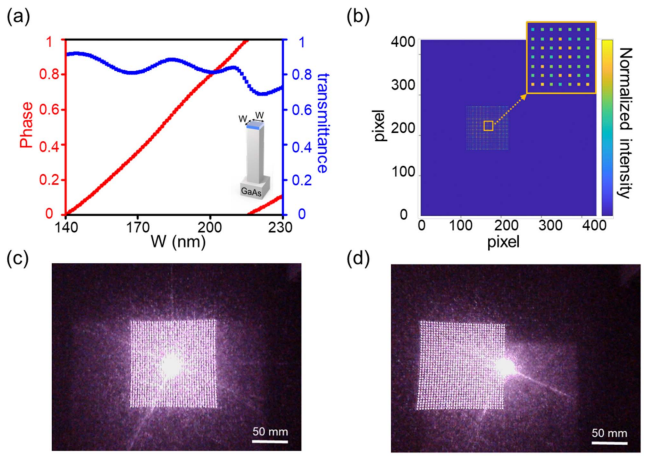

Fig. 3. (a) The graph illustrates the phase compensation and corresponding transmittance of propagation phase-based meta-atoms fabricated using GaAs material. (b) The schematic presents the design of a SL distribution with a FOV of 20° × 20° using the diffraction formula. (c) The experimental result of a multi-beam SL projection using a propagation phase-based meta-hologram. (d) Generation multi-beam SL projection with a customized FOV_x tailored from −20° to 0°.

to consider the tradeoff between the distance of adjacent pixel points and the dimensions of the reconstructed image Additionally, the imaging quality of the points must also be considered. Therefore, the pixel spacing between points in the multi-beam SL array is designed to be 3 (the sampling angle is 0.203°, [30]), the clarity of reconstructed light spots increases.

A. Propagation Phase Meta-Hologram

In our demonstration, we realized SL projection at 940 nm. Within the diffraction limit determined by the periodically arranged meta-atoms, we achieved arbitrary SL distributions at the pixel points. The propagation phase [31] is controlled by modulating the width of meta-atom, thereby altering the propagation path. First, to implement the multi-beam SL, we used square meta-atom made of Gallium Arsenide (GaAs) with varying widths. The aim is to achieve a complete 2π phase coverage while maintaining high transmittance conditions, realizing an effective phase control and the optimal performance in phase-based applications. The meta-atom height is 800 nm, and the pitch of meta-atom 330 nm is selected for its relatively high transmittance. The phase and transmittance for square meta-atoms with widths ranging from 140 nm to 230 nm were calculated using rigorous coupled-wave analysis (RCWA), as shown in Fig. 3(a). The meta-atoms exhibit transmittance ranging from approximately 70% to 90% while satisfying the phase requirements. To enable arbitrary beam control within FOV, the SL array achieves an overall FOV spanning 20° × 20°. Specifically, the FOV along the X-direction (FOV_x) is tailored from −20° to 0°, allowing for precise control over light distribution and deflection, as depicted in Fig. 3(b).

In the experimental setup, we utilized a commercial 940-nm PCSEL as the laser light source (L13395-04, Hamamatsu). The threshold current is around 200 mA with a slope efficiency of 0.495 W/A, and an output power of around 85 mW at 400 mA [30]. It provides excellent beam quality with an extremely small divergence angle, eliminating the need for additional lens assemblies and optical system for correction. This enables outstanding performance in the SL array generation system. The experimental realization of multi-beam SL projection with a FOV of 20° × 20° using a propagation phase-based meta-hologram as shown in Fig. 3(c).

Additionally, we have demonstrated multi-beam SL projection with customized FOV_x tailored from −20° to 0°, as shown in Fig. 3(d). The experimental findings demonstrate that the propagation phase-based meta-hologram facilitates the realization of multi-beam SL arrays. Nevertheless, this method is limited by the diffraction angle $\theta_{0\text{th}}$ determined by the periodic structural design.

B. Geometric Phase Meta-Hologram

We harness the geometric phase (Pancharatnam–Berry phase) to implement the holographic phase, thereby improve FOV imposed by the periodic structural design. To implement the computed phase, we first perform numerical calculations of the geometric phase meta-atoms. In this method, the meta-atoms are described using birefringent Jones matrices, with complex transmission coefficients representing the meta-atoms along the long ($\tilde{t}_L$) and short ($\tilde{t}_S$) axes. Under circular polarized light incidence, this can be described as follows:

$$M\frac{1}{\sqrt{2}}\begin{bmatrix}1\\ i\end{bmatrix} = \frac{1}{2}(\tilde{t}_L+\tilde{t}_S)\frac{1}{\sqrt{2}}\begin{bmatrix}1\\ i\end{bmatrix} + \frac{1}{2}e^{+i2\alpha}(\tilde{t}_L-\tilde{t}_S)\frac{1}{\sqrt{2}}\begin{bmatrix}1\\ -i\end{bmatrix} \tag{3}$$

$$M\frac{1}{\sqrt{2}}\begin{bmatrix}1\\ -i\end{bmatrix} = \frac{1}{2}e^{-i2\alpha}(\tilde{t}_L-\tilde{t}_S)\frac{1}{\sqrt{2}}\begin{bmatrix}1\\ i\end{bmatrix} + (\tilde{t}_L+\tilde{t}_S)\frac{1}{\sqrt{2}}\begin{bmatrix}1\\ -i\end{bmatrix} \tag{4}$$

where α represents the rotation angle of the meta-atom. Based on this equation, the resulting circular polarized light can have its phase determined by the rotation angle of the meta-atoms. Notably, the phase is modulated to twice the rotation angle of the meta-atoms, enabling arbitrary phase control. To achieve optimal meta-atoms, we aim to convert all incident circular polarized light into the opposite handedness of circular polarization. Considering the requirement to satisfy the condition $(\tilde{t}_L-\tilde{t}_S=0)$ for meta-atoms, achieving high polarization conversion efficiency is essential, as described by the following formula:

$$\text{PCE} = \frac{\left|\tilde{t}_L-\tilde{t}_S\right|^2}{4} \tag{5}$$

Herein, the meta-atoms were simulated using GaAs material of different lengths and widths, but all with a fixed height of 800 nm. The highest polarization conversion efficiency 79% has a length of 222 nm and a width of 127 nm by using RCWA optimization, as shown in Fig. 4(a). This set of meta-atom parameters was selected due to its highest polarization conversion efficiency, which enhances phase control capability. Furthermore, due to the

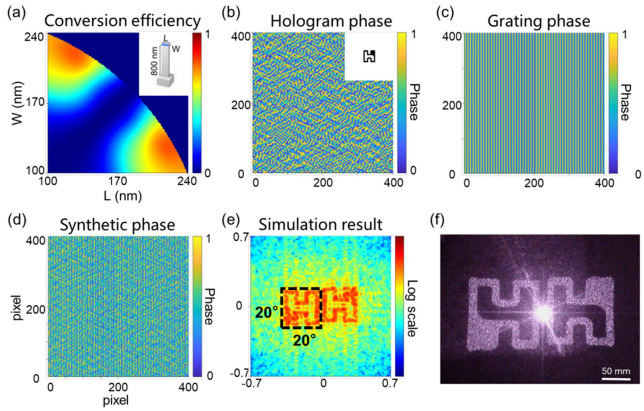

Fig. 4. (a) The graph presents the corresponding polarization conversion efficiency of various geometric phase meta-atoms. (b) The near-field phase distribution for the Hon Hai logo is combined with the (c) deflection phase distribution for separation. (d) Final synthetic phase. (e) The simulation result of Hon Hai logos meta-hologram (f) the experimental result of Hon Hai logos with the separated RCP and LCP components.

physical particularity of geometric phase, the phase distribution imparted to the RCP beam is ϕ_{RCP}, while the LCP beam obtains the opposite phase distribution, namely $\phi_{LCP} = -\phi_{RCP}$.

To harness the characteristics of geometric phase for holography, we first design the Hon Hai logo with a FOV of $20° \times 20°$. The near-field phase distribution for the Hon Hai logo is calculated by the aforesaid G-S algorithm as shown in Fig. 4(b). Leveraging the characteristics of geometric phase, we improve the FOV imposed by periodic structures. Incorporating a phase distribution capable of deflecting by 10° for separation (as depicted in Fig. 4(c)) onto the holographic image. The phase distribution for deflection can be described as:

$$\phi(x) = \frac{2\pi}{\lambda}(x \sin\theta \cos\varphi + y \sin\theta \sin\varphi) \tag{6}$$

where λ represents the wavelength, and θ and φ represent the diffraction angle and azimuth angle in spherical coordinates. We obtain the corresponding synthetic phase, which integrates both the holographic and deflection phase components, as illustrated in Fig. 4(d). Notably, this innovative approach utilizes a geometric phase metasurface to generate symmetric LCP and RCP far-field light patterns. At the opposite direction ($-10°$), it will project a completely rotated reconstructed image with opposite circular polarization state. The simulation of designed meta-hologram is performed by Finite-Difference Time-Domain (FDTD) method to calculate the geometric phase holography, showcasing the reconstructed image achieved through the geometric phase meta-hologram, as illustrated in Fig. 4(e). The simulation results demonstrate that the Hon Hai logos are projected at $+10°$ and $-10°$, revealing rotated images representing RCP and LCP, respectively. In Fig. 4(f), The experimental realization of the designed Hon Hai logos with the separated RCP and LCP components. The measurement results confirmed that the doubling of the FOV could be harnessed using geometric phase. Through analysis, it was successfully demonstrated that the original FOV range from $-10°$ to 10° was expanded to $-20°$ to 20°.

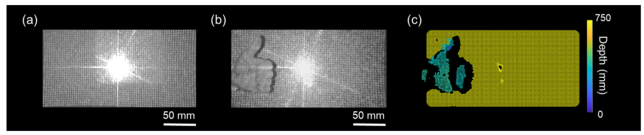

Fig. 5. (a) The experimental result of multi-beam SL with the separated RCP and LCP components. (b) The SL is projected onto the target capturing the hand gesture. (c) The reconstruction point cloud of the 3D depth sensing.

III. Performance of the Meta-Hologram Single-Shot Structured Light System

Based on the previously demonstrated SL with a specialized FOV, by incorporating a 10° deflection phase into the multi-beam SL phase, an impressive SL projection is generated using a geometric phase metasurface, with a FOV of $40° \times 20°$ twice as wide as the previous demonstration. The resulting output, consisting of intricate patterns with both RCP and LCP light, proposes an innovative approach to overcome the limited FOV. The measurement results are depicted in Fig. 5(a). The establishment of depth perception consists of three steps: 1) Computing image disparity using information from reference and target images, where a block matching algorithm is employed to generate the disparity image; 2) Calculating depth image through triangulation approximation method based on the analysis of the disparity image; 3) Ultimately, extracting depth information from the depth image and performing coordinate transformation to obtain the reconstructed point cloud image. For detailed methods used in reconstructing depth information in a single SL system, refer to previous work [32], [33], [34].

Based on Fig. 5(a) as the reference image of SL projection, the SL is projected onto the gesture to generate the deformation of SL, and its infrared image is captured as shown in Fig. 5(b). Finally, after extracting depth information and performing global coordinate transformation, the result of reconstructed point cloud gesture image is obtained as depicted in Fig. 5(c), confirming the way for advanced 3D sensing applications.

Furthermore, it is necessary to consider the reconstruction distance and beam divergence angle when demonstrating a multi-beam SL meta-hologram system. Specifically, maintaining a sufficient Fraunhofer diffraction distance is paramount for achieving high-quality holographic reconstruction, as this parameter directly impacts the clarity of the reconstructed image [30]. Additionally, the divergence angle of the employed laser source must also be carefully considered. A larger divergence angle leads to a decrease in power density, resulting in the dilution of output energy as the optical wave propagates. This ultimately limits the practical operating range of the system. Referring to and based on our previous research findings to satisfy this condition, the working distance needed to exceed 30 cm. Therefore, a better and clear recognition distance of 75 cm was selected.

Thus, we propose the use of a PCSEL as the light source for our meta-hologram system. The PCSEL offers inherent advantages that significantly enhance the system's performance and practicality. It provides excellent beam quality with an extremely small divergence angle, eliminating the need for additional

lens assemblies for correction. This characteristic ensures that the optical power remains concentrated over longer distances, extending the effective range of the holographic reconstruction. Moreover, the PCSEL's compact size, low power consumption, and high efficiency make it an ideal choice for integration into portable and energy-efficient devices, further expanding the potential applications of our meta-hologram system.

IV. Conclusion

In conclusion, we have presented a clear and effective approach that leverages geometric phase metasurfaces and photonic crystal surface-emitting lasers for holographic image reconstruction and 3D sensing. Compared with the existing vertical cavity surface emitting lasers optical system, we using photonic crystal surface-emitting lasers as the light source. Their high beam collimation eliminates the need for lenses to reshape the light, thereby reducing costs and system complexity. This approach effectively addresses the output limitations and divergence angle issues associated with vertical cavity surface emitting lasers. Numerical simulations were conducted to reconstruct the corresponding images of the Hon Hai logo and the multi-beam structured light array, demonstrating the capability for arbitrary light control. Herein, the demonstrated technique based on geometric phase offers unique advantages in image reconstruction. By employing a rigorous design to precisely define the wavefront phase and incorporate additional deflection phases, we have achieved superior performance. The experimental results show that geometric phase meta-holograms designed using this approach can surpass the diffraction limit imposed by the pixel size of nanostructures, resulting in a reconstructed image with a field of view twice as wide, consisting of both right-circular polarization and left-circular polarization states. Moreover, we have explored the potential of the multi-beam structured light metasurface for 3D spatial sensing applications. By operating at a wavelength of 940 nm and a distance of 75 cm, we have successfully demonstrated structured light depth sensing using meta-holography. The integration of photonic crystal surface-emitting lasers has been crucial in achieving this compact integrated solution, owing to their easy integration and high beam quality. This combination holds significant promise for spatial perception and depth sensing applications. The potential for system miniaturization and customization suggests such a technique has a bright future, with promising developments on the horizon.

Acknowledgment

The authors acknowledge the Semiconductor Research Center, Hon Hai Research Institute for their technical support. We also acknowledge Prof. Tien-Chang Lu and Prof. Edward Yi Chang for their technical discussion.

References

[1] M. Yoshida et al., "Photonic-crystal lasers with high-quality narrow-divergence symmetric beams and their application to LiDAR," *J. Phys. Photon.*, vol. 3, no. 2, Apr. 2021, Art. no. 022006, doi: 10.1088/2515-7647/abea06.

[2] H. Pahlevaninezhad et al., "Nano-optic endoscope for high-resolution optical coherence tomography in vivo," *Nature Photon.*, vol. 12, no. 9, pp. 540–547, Sep. 2018, doi: 10.1038/s41566-018-0224-2.

[3] S.-P. Yang, Y.-H. Seo, J.-B. Kim, H. Kim, and K.-H. Jeong, "Optical MEMS devices for compact 3D surface imaging cameras," *Micro Nano Syst. Lett.*, vol. 7, no. 1, Dec. 2019, Art. no. 8, doi: 10.1186/s40486-019-0087-4.

[4] Z. Song, S. Tang, F. Gu, C. Shi, and J. Feng, "DOE-based structured-light method for accurate 3D sensing," *Opt. Lasers Eng.*, vol. 120, pp. 21–30, Sep. 2019, doi: 10.1016/j.optlaseng.2019.02.009.

[5] F. Gu, H. Cao, Z. Song, P. Xie, J. Zhao, and J. Liu, "Dot-coded structured light for accurate and robust 3D reconstruction," *Appl. Opt.*, vol. 59, no. 33, Nov. 2020, Art. no. 10574, doi: 10.1364/AO.403624.

[6] N. Yu and F. Capasso, "Flat optics with designer metasurfaces," *Nature Mater.*, vol. 13, no. 2, pp. 139–150, Feb. 2014, doi: 10.1038/nmat3839.

[7] J. P. Balthasar Mueller, N. A. Rubin, R. C. Devlin, B. Groever, and F. Capasso, "Metasurface polarization optics: Independent phase control of arbitrary orthogonal states of polarization," *Phys. Rev. Lett.*, vol. 118, no. 11, Mar. 2017, Art. no. 113901, doi: 10.1103/PhysRevLett.118.113901.

[8] Z.-L. Deng et al., "Full-color complex-amplitude vectorial holograms based on multi-freedom metasurfaces," *Adv. Funct. Mater.*, vol. 30, no. 21, May 2020, Art. no. 1910610, doi: 10.1002/adfm.201910610.

[9] Z.-L. Deng et al., "Poincaré sphere trajectory encoding metasurfaces based on generalized Malus' law," *Nature Commun.*, vol. 15, no. 1, Mar. 2024, Art. no. 2380, doi: 10.1038/s41467-024-46758-y.

[10] K. Iga, F. Koyama, and S. Kinoshita, "Surface emitting semiconductor lasers," *IEEE J. Quantum Electron.*, vol. 24, no. 9, pp. 1845–1855, Sep. 1988, doi: 10.1109/3.7126.

[11] K. Iga, "Vertical-cavity surface-emitting laser: Its conception and evolution," *Jpn. J. Appl. Phys.*, vol. 47, no. 1R, Jan. 2008, Art. no. 1, doi: 10.1143/JJAP.47.1.

[12] K. Iga, "Vertical-cavity surface-emitting laser (VCSEL)," *Proc. IEEE*, vol. 101, no. 10, pp. 2229–2233, Oct. 2013, doi: 10.1109/JPROC.2013.2275016.

[13] Y.-Y. Xie et al., "Metasurface-integrated vertical cavity surface-emitting lasers for programmable directional lasing emissions," *Nature Nanotechnol.*, vol. 15, no. 2, pp. 125–130, Feb. 2020, doi: 10.1038/s41565-019-0611-y.

[14] Q. Wang et al., "On-chip generation of structured light based on metasurface optoelectronic integration," *Laser Photon. Rev.*, vol. 15, no. 3, Mar. 2021, Art. no. 2000385, doi: 10.1002/lpor.202000385.

[15] P.-N. Ni, P. Fu, P.-P. Chen, C. Xu, Y.-Y. Xie, and P. Genevet, "Spin-decoupling of vertical cavity surface-emitting lasers with complete phase modulation using on-chip integrated Jones matrix metasurfaces," *Nature Commun.*, vol. 13, no. 1, Dec. 2022, Art. no. 7795, doi: 10.1038/s41467-022-34977-0.

[16] D. Wen, J. Meng, J. J. Cadusch, and K. B. Crozier, "VCSELs with on-facet metasurfaces for polarization state generation and detection," *Adv. Opt. Mater.*, vol. 9, no. 9, May 2021, Art. no. 2001780, doi: 10.1002/adom.202001780.

[17] M. Imada, A. Chutinan, S. Noda, and M. Mochizuki, "Multidirectionally distributed feedback photonic crystal lasers," *Phys. Rev. B*, vol. 65, no. 19, Apr. 2002, Art. no. 195306, doi: 10.1103/PhysRevB.65.195306.

[18] K. Hirose, Y. Liang, Y. Kurosaka, A. Watanabe, T. Sugiyama, and S. Noda, "Watt-class high-power, high-beam-quality photonic-crystal lasers," *Nature Photon.*, vol. 8, no. 5, pp. 406–411, May 2014, doi: 10.1038/nphoton.2014.75.

[19] K. Ishizaki, M. De Zoysa, and S. Noda, "Progress in photonic-crystal surface-emitting lasers," *Photonics*, vol. 6, no. 3, Aug. 2019, Art. no. 96, doi: 10.3390/photonics6030096.

[20] Y.-H. Hong et al., "Progress of photonic-crystal surface-emitting lasers: A paradigm shift in LiDAR application," *Crystals*, vol. 12, no. 6, Jun. 2022, Art. no. 800, doi: 10.3390/cryst12060800.

[21] Y.-W. Huang et al., "Aluminum plasmonic multicolor meta-hologram," *Nano Lett.*, vol. 15, no. 5, pp. 3122–3127, May 2015, doi: 10.1021/acs.nanolett.5b00184.

[22] W.-C. Hsu, C.-H. Chang, Y.-H. Hong, H.-C. Kuo, and Y.-W. Huang, "Compact structured light generation based on meta-hologram PCSEL integration," *Discover Nano*, vol. 18, no. 1, Jun. 2023, Art. no. 87, doi: 10.1186/s11671-023-03866-w.

[23] G. Zheng, H. Mühlenbernd, M. Kenney, G. Li, T. Zentgraf, and S. Zhang, "Metasurface holograms reaching 80% efficiency," *Nature Nanotechnol.*, vol. 10, no. 4, pp. 308–312, Apr. 2015, doi: 10.1038/nnano.2015.2.

[24] K. Khoshelham and S. O. Elberink, "Accuracy and resolution of kinect depth data for indoor mapping applications," *Sensors*, vol. 12, no. 2, pp. 1437–1454, Feb. 2012, doi: 10.3390/s120201437.

[25] H. Nguyen, Z. Wang, P. Jones, and B. Zhao, "3D shape, deformation, and vibration measurements using infrared Kinect sensors and digital image correlation," *Appl. Opt.*, vol. 56, no. 32, pp. 9030–9037, Nov. 2017, doi: 10.1364/AO.56.009030.

[26] M. Khorasaninejad and K. B. Crozier, "Silicon nanofin grating as a miniature chirality-distinguishing beam-splitter," *Nature Commun.*, vol. 5, no. 1, Nov. 2014, Art. no. 5386, doi: 10.1038/ncomms6386.

[27] M. Khorasaninejad, W. T. Chen, R. C. Devlin, J. Oh, A. Y. Zhu, and F. Capasso, "Metalenses at visible wavelengths: Diffraction-limited focusing and subwavelength resolution imaging," *Science*, vol. 352, no. 6290, pp. 1190–1194, Jun. 2016, doi: 10.1126/science.aaf6644.

[28] R. W. Gerchberg, "A practical algorithm for the determination of plane from image and diffraction pictures," *Optik*, vol. 35, no. 2, pp. 237–246, 1972.

[29] G. Huang et al., "Generalizing the Gerchberg–Saxton algorithm for retrieving complex optical transmission matrices," *Photon. Res.*, vol. 9, no. 1, pp. 34–42, Jan. 2021, doi: 10.1364/PRJ.406010.

[30] W.-C. Hsu, C.-H. Chang, Y.-H. Hong, H.-C. Kuo, and Y.-W. Huang, "Metasurface- and PCSEL-based structured light for monocular depth perception and facial recognition," *Nano Lett.*, vol. 24, no. 5, pp. 1808–1815, Feb. 2024, doi: 10.1021/acs.nanolett.3c05002.

[31] M. Khorasaninejad et al., "Polarization-insensitive metalenses at visible wavelengths," *Nano Lett.*, vol. 16, no. 11, pp. 7229–7234, Nov. 2016, doi: 10.1021/acs.nanolett.6b03626.

[32] Z. Zhang, "A flexible new technique for camera calibration," *IEEE Trans. Pattern Anal. Mach. Intell.*, vol. 22, no. 11, pp. 1330–1334, Nov. 2000, doi: 10.1109/34.888718.

[33] G. Wang, X. Yin, X. Pei, and C. Shi, "Depth estimation for speckle projection system using progressive reliable points growing matching," *Appl. Opt.*, vol. 52, no. 3, pp. 516–524, Jan. 2013, doi: 10.1364/AO.52.000516.

[34] M. Donlic, T. Petkovic, and T. Pribanic, "On tablet 3D structured light reconstruction and registration," in *Proc. 2017 IEEE Int. Conf. Comput. Vis. Workshops*, Venice, Italy, 2017, pp. 2462–2471, doi: 10.1109/ICCVW.2017.290.